Computer-Controlled System for the Investigation of the Flow behind Wings

Z. M. El-Ramly* and W. J. Rainbird†
Carleton University, Ottawa, Canada

A completely computer-controlled wind-tunnel test facility designed for measurements of the vortical flowfield behind a lifting swept-back wing is described. The vortex generator model is a pressure-plotted root-mounted half-wing. To avoid unrepresentative end effects, distributed wingroot suction is applied over an area surrounding the root chord. The detailed design and calibration of the root suction system is discussed. Flowfield measurements were made using a precalibrated non-nulling blunted conical five-hole probe. The use of the conical head made probe calibration over a wide flow angle range, and the consequent memory required to store the calibration data, a simple task. The program developed can calculate and plot, on-line, the three components of velocity and vorticity, the total pressure loss coefficient, and the circulation distribution. Because of the speed and large capability for data handling, detailed flow surveys behind the wing were made feasible. As a result of these automated flowfield measurements, it was possible to account for almost all of the vorticity shed from the wing. The rollup is neither complete nor axisymmetric in form within five wingspans downstream.

I. Introduction

A CAREFUL study of the literature on the trailing vortex problem (see for example Refs. 1 and 2) has revealed to the authors that an accurate and complete set of wind-tunnel measurements would be of great help in understanding the initial formation and rollup of trailing vortices. An experimental setup was designed and built which allows the measurements of the detailed loading on the main wing, the mean properties of the induced flowfield, and the induced rolling moment on representative trailing wings. Because of the care taken in making the measurement and in correcting for the facility flow disturbances, some features of the induced flowfield were found which probably would not have been evident without the added accuracy of the measurements. For example, it was found that the shear layers separating from the wing were effectively rolled up (at a 5 span station downstream of the mean ¼ chord), but not in axisymmetric form. Also, it was found that only about 45% of the wingroot circulation appears around a concentrated vortex core (see Refs. 3 and 4). A conclusion from these results is that detailed flow surveys must be obtained, in contrast to a single scan through the vortex center if the flow is axisymmetric. The amount of data to be collected and the data reduction involved dictated the adoption of a fully computer-controlled system with on-line data reduction. This paper attempts to describe the precautions taken in designing the system, the technique of data reduction and interference correction, and the computer-controlled system.

II. Experimental Setup

The tunnel under consideration is a 20×30 in. low-speed return circuit wind tunnel at Carleton University. For the trailing vortex program the test section, which is normally 6-ft long, has been extended by adding an additional 16 ft of working section in place of the first diffuser of the wind tunnel. Because trailing vortices are axial pressure gradient sensitive, essentially zero gradient has been achieved in the empty tunnel by a combination of divergence of the top and bottom walls and small 45° corner fillets. Figure 1 shows a schematic of the working section layout, and Table 1 gives the overall dimensions of the wings used. The vortex-generating half-wing (herein called main wing) is sidewall-mounted on an incidence gear which also serves as the resistive side of a root suction system. The main wing and its root suction system (suction box) can be removed easily, and the working section sidewall replaced, to run reference "empty tunnel" tests.

Flowfield measurements (local total pressure and three orthogonal mean velocity components) were made using a precalibrated, non-nulling, blunted conical, five-hole probe. The probe is attached to an x-y traversing mechanism which is mounted on continuous rails on the working section sidewall. The rails are mounted such that the traversing mechanism slides, manually, parallel to the test section centerline. A device (see Fig. 2) that could be mounted upstream of the probe during setups helps in physically defining the centerline of the test section and in probe alignment. This device is needed especially because of the divergence of the test section.

The intercepting trailing wings (chosen to be representative of a light aircraft and medium commercial transport) are sting-mounted from a floor-mounted traversing strut. The rolling moment induced on these wings is measured on a simple strain-gauged cantilever element roll balance. Calibration of the combined roll balance and readout display system is made statically using a calibration arm and dead

Table 1 Wing dimensions

Dimension	Main (half-) wing	Trailing wings	
		Straight wing	Sweptback wing
Span	21.0 in. (×2)	10.0 in.	20.0 in.
Relative span	1	0.24	0.48
Average chord	6.00 in.	1.33 in.	2.35 in.
Aspect ratio	7.0	7.5	8.5
Taper ratio	⅓	1	⅓
Sweepback (¼c)	35°	0°	35°
Wing twist	0°	0°	0°
Wing section	12%, symmetrical	NACA 64_2-015	NACA 64_2-015
Tip form	half body	square cut	square cut

Presented at the AIAA 9th Aerodynamic Testing Conference, Arlington, Texas, June 9, 1976 (in bound volume of Conference papers, no paper number); submitted June 29, 1976; revision received March 9, 1977.

Index categories: Testing, Flight and Ground; Jets, Wakes, and Viscid-Inviscid Flow Interactions.

*Research Associate, Dept. of Mechanical and Aeronautical Engineering. Member AIAA.

†Professor of Engineering, Dept. of Mechanical and Aeronautical Engineering. Member AIAA.

weight, after each test. The linearity of the system is better than 1%; hysteresis is also less than 1% of full scale.

Complete details of the system can be found in Ref. 4; details of simulated jet engines, which can be mounted on the main wing, are given in Ref. 5. However, some details of the design and calibration of the system, which are thought to be of interest, will be discussed in the following.

Wingroot Suction

The main (half-) wing is sidewall-mounted to facilitate the supply of the high-pressure air, simulating the jet engine's exhaust, and the connection of the surface pressure plotting tubes. Unrepresentative end effects could result from the interaction of the wing pressure field and the sidewall boundary layer. To avoid these effects, distributed suction is applied over an area surrounding the root. The criterion used for calculating the suction requirement is that presented in Ref. 6 (the removal of one to three times the approaching turbulent boundary-layer deficit mass flow). The suction box pressure coefficient is determined from the requirement that the suction flow is not to reverse locally. Hence the pressure behind the suction plate must be lower than the lowest pressure in the flowfield near the wingroot at the highest lift coefficient used. ¼-in. thick grade 'd' Porosint (Sintered Products Ltd., Hamilton Road, Sutton-in-Ashfield, England) sintered bronze was found to have a resistance that should give the required flow rate over the suction area (15.5 × 14 in.) at the required pressure loss.

The suction system was calibrated, in the wind tunnel, before the main wing was mounted. The objective of the calibration was to establish the minimum flow rate required to reduce the boundary-layer thickness to its minimum value, governed by the sintered bronze surface roughness, while still maintaining the required pressure loss across the plate. Figure 3 shows the results of the calibration; the momentum thickness was obtained from pitot tube rake measurements just downstream of the suction plate. It is clear from the figure that increasing the flow rate to more than about 200 cfm ($V_s/V_\infty = 0.013$) does not result in any appreciable decrease in the momentum thickness of the downstream boundary layer. However, the flow rate has to be increased to 240 cfm ($V_s/V_\infty = 0.016$) to achieve the required suction box coefficient. This flow rate is equivalent to about 1.8 times the approaching boundary-layer deficit mass flow (and incidentally is about 0.5% of the working section flow rate). In defining "undisturbed" working section freestream velocity (dynamic pressure) average values upstream and downstream of the suction box were used.

The effect of the root suction on main wing spanwise loading is shown in Fig. 4 (the values of the local lift coefficient were obtained from integration of the chordwise loading at different measuring stations). The dip in the loading near the root, without suction, is critical to trailing vortex measurements, since it could result in shedding of secondary vorticity of opposite sign to the main tip vortex.

Transition Fixing on Main and Trailing Wings

Because of the relatively low chord Reynolds number attainable in the test facility, the nature of the boundary layer and its separation is of particular concern. For the main wing, the Reynolds number based on mean chord, R_c, is 0.5×10^6 at the tunnel maximum speed of 175 fps, i.e., about 1/50 of full scale. Oil dot flow visualization revealed that, on the upper surface of the main wing, a short laminar separation bubble is present, at about 5-10%c from the leading edge. This separation bubble is caused by the large leading radius of the peaky section used and results in a turbulent boundary layer downstream of reattachment. This turbulent state of the

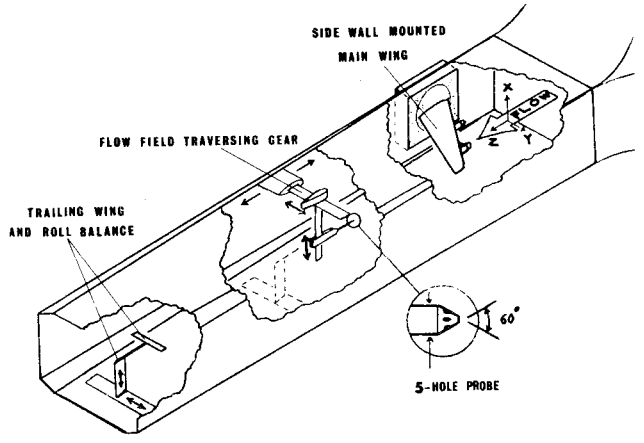

Fig. 1 Isometric sketch of working section.

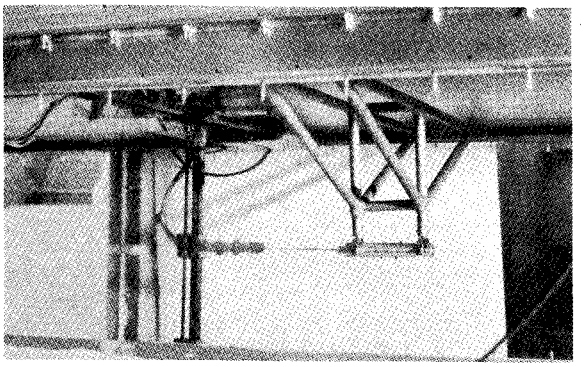

Fig. 2 Photograph showing centerline locating device.

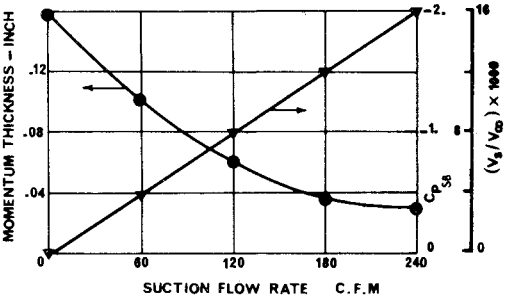

Fig. 3 Suction system calibration at maximum wind-tunnel speed (175 fps).

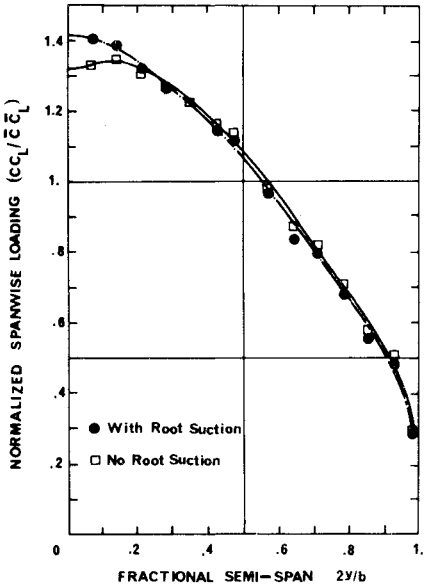

Fig. 4 Effect of root suction on wing spanwise loading.

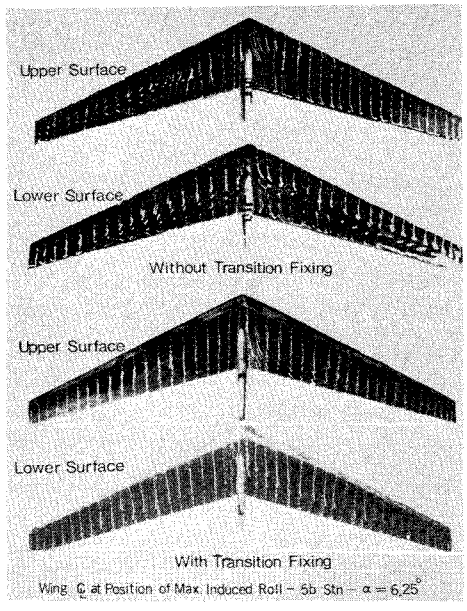

Fig. 5 Surface flow visualization on swept trailing wing.

boundary layer was confirmed by limited hot-wire measurements. On the lower surface of the wing, the hot-wire measurements suggested a turbulent boundary layer for angles of attack larger than 6.25°, probably as a result of sweep instability. However, at smaller angles of attack, laminar separation near the trailing edge necessitated fixing transition on the lower surface. This was done using a band of ballatini balls (0.0054 in.) of 0.05-in. width placed 0.6 in. downstream of the leading edge.

For the two trailing wings the chord Reynolds numbers were 1.3 and 2.4×10^5 for the straight and swept wings, respectively. Induced rolling moments made without transition fixing were very sensitive to trailing wing incidence (wings are set at nominally zero angle of attack). By fixing transition (using sand band strips, 0.0057-0.0072 in., to 15% chord, on both surfaces) their sensitive behavior to incidence was eliminated and more repeatable results made possible. Figure 5 shows surface flow visualization on the swept trailing wings in the wake of the generating wing, at a moderate lift coefficient of 0.46, $\alpha=6.25°$, with and without transition fixing. The importance of fixing the transition is quite clear from the flow visualization in that spurious laminar boundary-layer separations are eliminated.

Five-Hole Pressure Probe

The probe used is a blunted conical head five-hole probe 0.093-in. o.d., including a cone angle of 60° (see Fig. 6). The peripheral tubes are numbered 1 to 4, and the center tube is 5. The pressures that they sense were referenced to a reference contraction static pressure p_c. Five variable capacitance differential pressure transducers were used for measuring these pressure differences. The transducers have a range of ±0.5 psid, or about twice the maximum test section dynamic head, and give a nominal output of ±2.5 Vdc.

The technique used for calibrating the probe in a uniform parallel flow is basically that of Wicken,[7] in which flow angularity is expressed in probe axes, namely roll and misalignment angles. The dimensionless parameters used are defined in the following way:

$$Q=(p_2-p_1)/p_5-p_{av}) \quad \text{(pitch parameter)}$$

$$R=(p_3-p_4)/(p_5-p_{av}) \quad \text{(yaw parameter)}$$

$$C_p=(p_{5_0}-p_5)/\tfrac{1}{2}\rho V^2 \quad \text{(total pressure parameter)}$$

$$P_d=(p_5-p_{av})/\tfrac{1}{2}\rho V^2 \quad \text{(dynamic head parameter)}$$

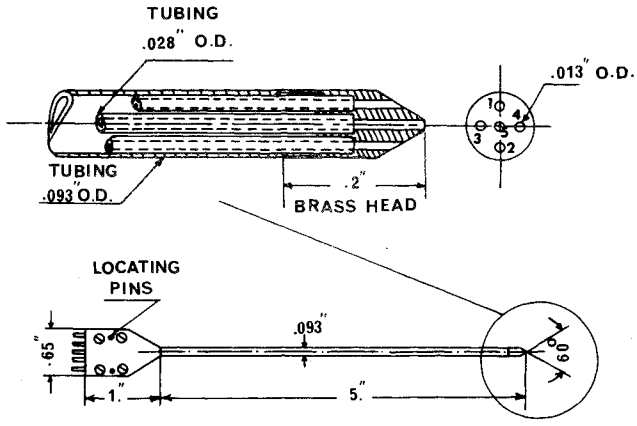

Fig. 6 Detail drawing of five-hole probe.

where $(p_{av}-p_c)=(p_1+p_2+p_3+p_4-4p_c)/4$ and p_{5_0} is the local total pressure.

The flow misalignment angle θ which is defined as the angle the velocity vector makes with the probe axis, and the roll angle ϕ, the angle the velocity and the probe axis plane make with a reference plane passing through the probe axis, can be calculated from the pitch α and yaw γ angles from the relations $\cos\theta=\cos\alpha\cdot\cos\gamma$ and $\tan\phi=\sin\gamma\cdot\cos\alpha/\sin\alpha$.

The calibration data are presented in Figs. 7a-7d; a satisfactory collapse with θ and ϕ is clear up to θ slightly higher than 30° (half the cone angle). Furthermore, the data for the four quadrants could be reduced or collapsed to one set (after allowance for a zero roll angle) with a small sacrifice in accuracy. When a least-squares technique was used to fit a polynomial to the data, the highest order required was always less than four. The use of the blunted conical head has eliminated the cyclic variation of the dynamic pressure parameter P_d with roll angle, as in Wicken's case for five-hole yaw meters composed of discrete tubes with a pyramidal face. As a result, the calibration of the probe is reduced to a set of four equations for each quadrant.

A major advantage in using the five-hole probe for flowfield measurements is the availability of the local total pressure. The regions of low total pressure define the lossy or viscous areas of the flow during measurements, which otherwise would not be easily identifiable except, maybe, after analyzing the results.

By feeding calibration pressure differences back into the data reduction program it is possible to assess the overall accuracy. The accuracy of the calibration decreases as θ increases. For $\theta<10°$ the accuracy in determining the local total pressure is better than 0.3% of the freestream dynamic head, the local velocity is better than 0.2% of the freestream velocity, and θ is within 0.5°. For $20°<\theta<30°$ the accuracy drops to 4% q_∞ in the total pressure, 2.5% V_∞ in local velocity, and 2° in θ. The accuracy in the roll angle ϕ is within 2°, irrespective to the value of θ. These quoted accuracies include calibration setup and measurements error; the fitted curves to the calibration data are probably more adequate than claimed. During actual flowfield measurements the misalignment angle θ seldom exceeded 15°; consequently, it can be claimed that the accuracy in measuring the flowfield velocity is better than 1% V_∞, and that the total pressure loss coefficient is accurate to within 0.005.

Empty-Tunnel Correction

There are three possible sources of error in the five-hole probe measurements. These are: 1) working section mean flow nonuniformities, 2) zero errors in setting the probe position and direction, and 3) upstream flow disturbances of probe holder and traversing mechanism. The working section has mean flow nonuniformities, within ±0.1°, and total pressure nonuniformities within 0.5% of the freestream

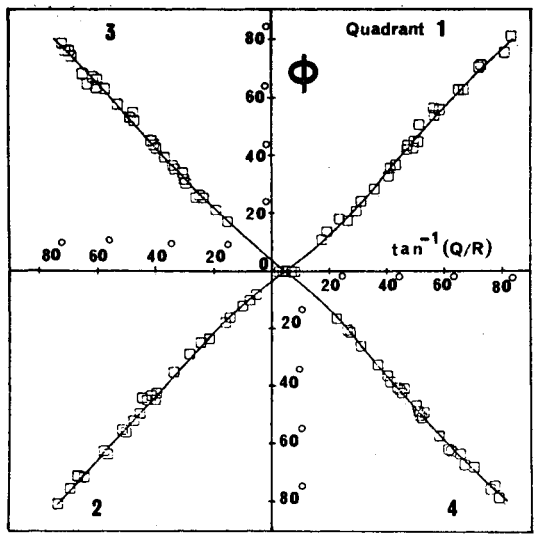

a) Variation of roll angle ϕ with $\tan^{-1}(Q/R)$

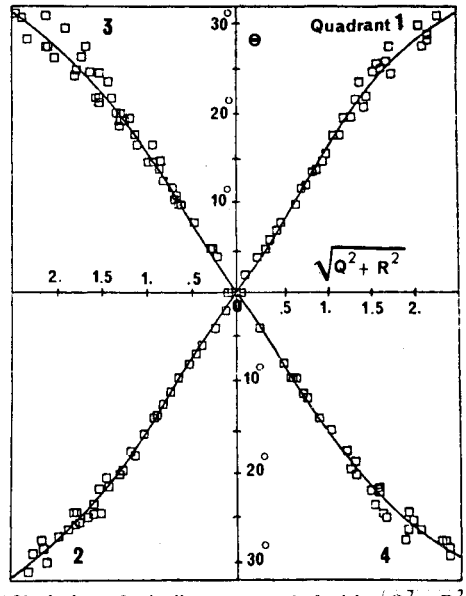

b) Variation of misalignment angle θ with $\sqrt{Q^2+R^2}$

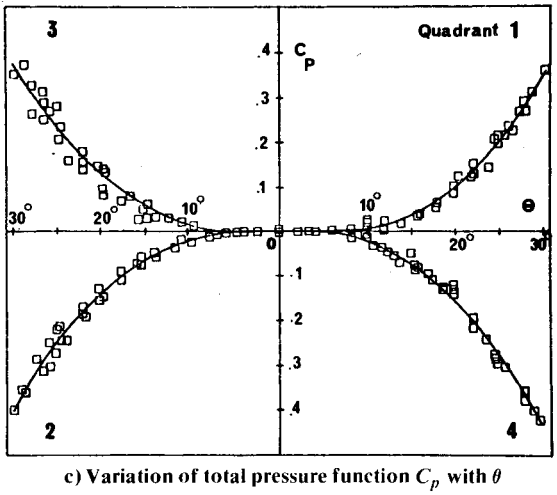

c) Variation of total pressure function C_p with θ

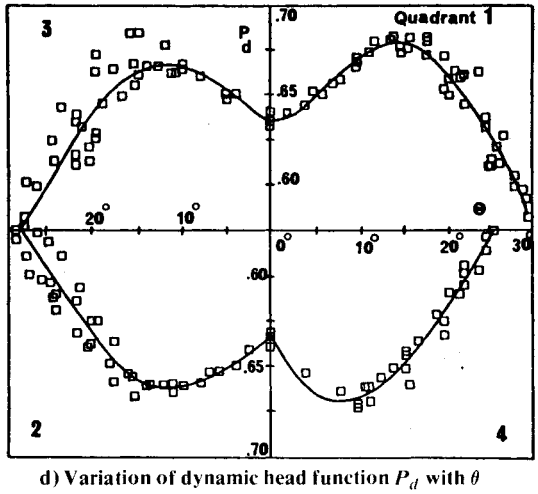

d) Variation of dynamic head function P_d with θ

Fig. 7 Probe calibration.

dynamic head. The five-hole probe, if required, could be set as accurate as $\pm 0.1°$ in both pitch and yaw. To minimize traversing mechanism upstream effects on the probe, a long stem is used (5-in. long). The probe is mounted on an aerodynamically shaped holder that extended another 5-in. upstream. The horizontal and vertical drives are housed in aerofoil shaped fairings with t/c about 0.15 and $t<2.0$ in. Still, the probe detected some upstream disturbances from the traversing mechanism. Figure 8 shows the relative variation of the static pressure with position for an empty tunnel. Measurements made with a large pitot-static tube, with the traversing mechanism removed, show static pressure coefficient nonuniformities of less than 0.005. The apparent nonuniformities measured with the five-hole probe, mounted on the traversing mechanism, are as high as 0.05. The static pressure profile indicates that the disturbances are coming from the vertical drive housing, which travels laterally with the probe.

To remove the traversing mechanism upstream effects, together with tunnel flow nonuniformities and any possible probe zero setting error, the empty-tunnel flow is surveyed at each downstream station after measurements with the vortex-generating wing present have been completed. After correction, the residual nonuniformities, as judged from scatter in the data, are less than $0.003V_\infty$ for V_x, V_y, and V_z, and less than $0.006q_\infty$ for p_0. It is worthwhile mentioning that traverses always are made in the same direction, laterally and vertically, thus eliminating any possible yaw or pitch resulting from backlash in the system and improving the repeatability of probe position. Accurate, zero directional setting of the probe consequently is not required, since small misalignment will be removed in the empty-tunnel correction.

For the rolling moment measurements on the trailing wings an empty-tunnel measurement also was made to remove any nonzero induced rolling moment as a result of machining nonuniformities of the wings or residual swirl in the empty working section flow. The empty-tunnel correction sometimes amounted to more than 10% of the maximum induced rolling moment due to the vortex and should stress the importance of the correction.

Vortex Meander

Reference 8 reports that large-scale wind-tunnel turbulence can result in a distorted vortex path or vortex meander (i.e., low-frequency movement). However, in our experimental setup, and following the 12:1 contraction with three $k=1.6$ screens, the flow in the working section has a streamwise component of turbulence of less than 0.2%. Measurements made using two total pressure probes, designed to have a matched response up to 100 Hz, showed that vortex meander

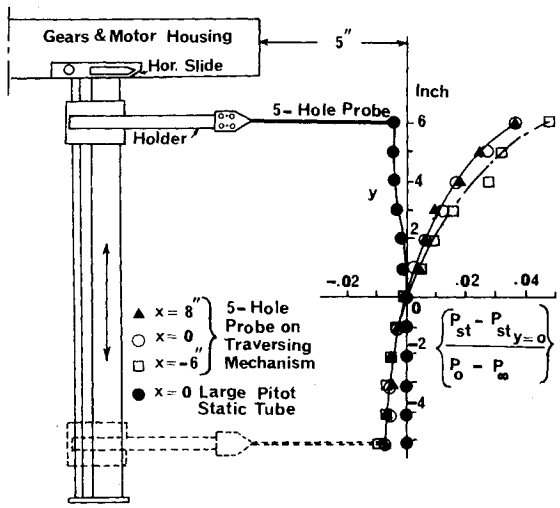

Fig. 8 Relative variation of static pressure coefficient with position.

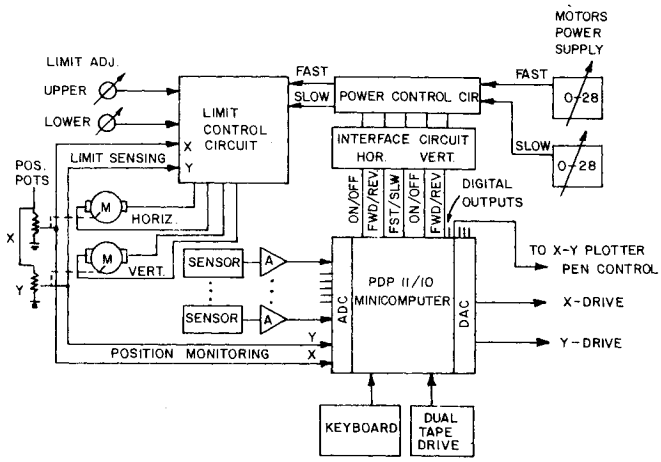

Fig. 9 Control system diagram.

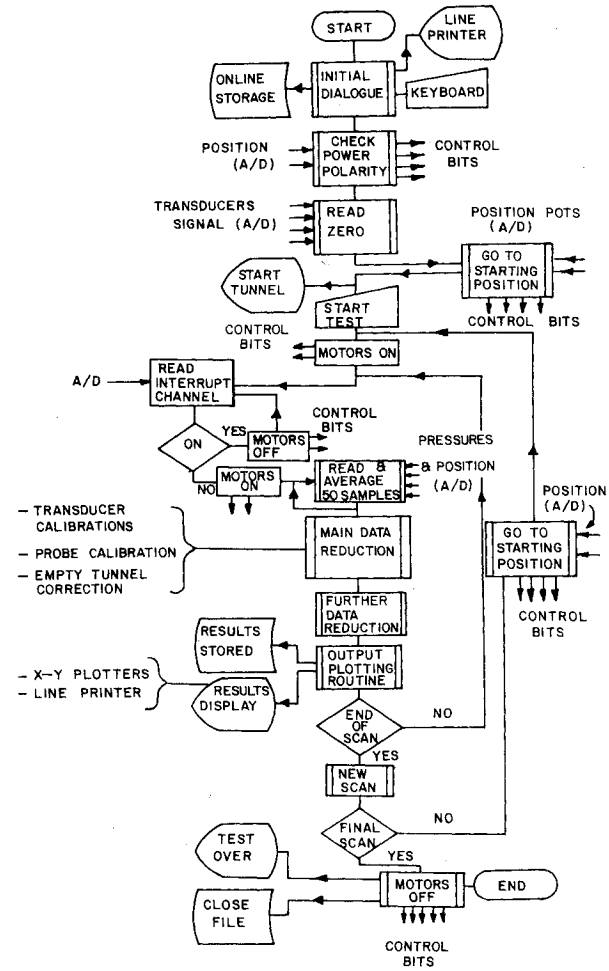

Fig. 10 Program flow chart.

is spatially very small (less than 0.25 in. with a main wing semispan of 21 in.).

The Computer-Controlled System

The computer used to control the system is a Digital PDP 11/10 with extended 24K memory. The computer is equipped with 16 channels of analog-to-digital A/D converters, 2 channels of digital-to-analog D/A converters, and a 16-word digital output. A fast decwriter II (300 characters/min) is used with the computer as well as a dual magnetic-type cassette drive system. Figure 9 shows a diagram of the computer and control system.

Six channels of the A/D converter are used to monitor the five-pressure differences from the five-hole probe and the "speed" sensing pressure difference. The A/D converters have an input range of ± 2.5 V and a resolution of 5 mV. To obtain the maximum resolution out of the system the signal from the pressure transducers first is amplified so that the maximum input to the A/D converters is close to 2.5 V. The transducers have a resolution of 0.1% q_∞, and the accuracy in measuring the pressure is determined largely by the digitization process.

The lateral and vertical positions of the probe are monitored using two position potentiometers (ten turns, 0.01% resolution). The potentiometers are supplied with 2.5 V as a reference and are geared to the corresponding lead screws. The output signals of the potentiometers are connected to two channels of the A/D converter; the resolution of 5 mV corresponds to 0.050-in. travel. The mechanical backlash in the system is less than 0.020 in., and again the accuracy in measuring the position is determined by the digitization process. Seven bits of the 16-word digital output are used to control the power supply for the lateral and vertical scanning motors, on/off, direction, and speed control. The slow speed, used for scanning, is determined by the probe response, since the computer has a very high read rate (less than 50 μsec per A/D converter channel). For the five-hole probe used, a speed of 1 in./min is slow enough to avoid lag effects in the steepest gradient near the vortex core. Fifty scans through the eight A/D converter channels are taken and averaged for each data point to remove high-frequency noise and improve resolution. Still, at a scanning rate of the probe of 1 in./min it is possible to collect data at 0.07-in. intervals, including data reduction and plotting. A fast speed is used to return the probe to a new position, since scanning is always done in the same direction, laterally and vertically, to avoid possible backlash effects. A control system, with adjustable limits, is used in series with the computer. The system monitors the position of the probe and shuts off the power supply if the probe reaches the preset limits. This control system is a safeguard against program and human errors.

A simplified flow chart of the program is shown in Fig. 10. The program starts with an initial dialog in which the test conditions, start and terminal positions, scanning direction, and increment are specified. The program then checks the polarity of the power supply to the motors, and reads the wind off zeroes of channels monitoring the transducers. A subroutine that outputs the control bits to the power supply then brings the probe to the starting position. Actually the subroutine will overshoot the position by a small amount then approach the starting point, slowly, in the scanning direction. In this way the backlash in the system is absorbed before

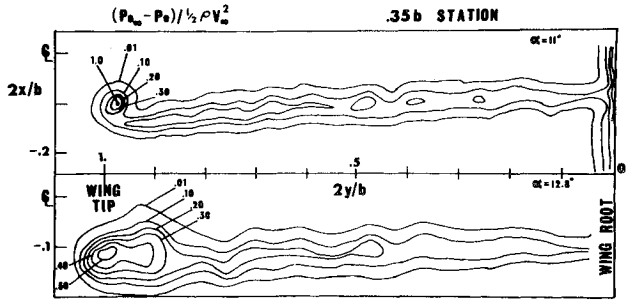

Fig. 11 Contours of equal total pressure loss coefficient: $(P_{0_\infty} - P_0)/\frac{1}{2}\rho V_\infty^2$ – 0.35b station.

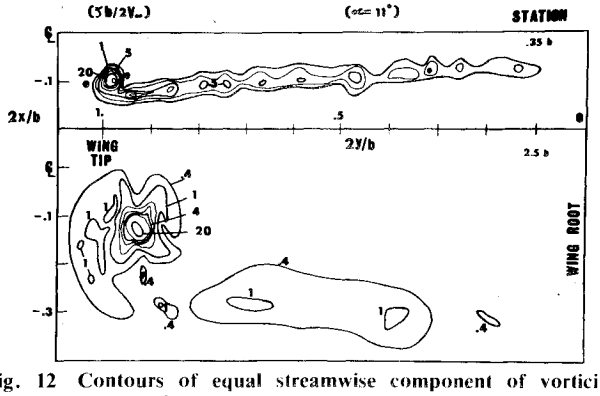

Fig. 12 Contours of equal streamwise component of vorticity, $\zeta b/2V_\infty$, for $\alpha = 11°$.

starting the measurements. After the starting point is reached a message is printed to turn the wind tunnel on. No further supervision of the system is required after that except when the test is completed or the magnetic tape cassette is full (about 2 hr, during which more than 800 data points are collected). The rest of the program is easy to follow from the flow chart and will not be discussed further here.

There is no need for precise control of the wind-tunnel speed since it is monitored continuously and used as a non-dimensionalizing parameter. However, plans are being made to computer control the tunnel operation so it could be turned off during probe return, for air temperature control and energy conservation reasons. The return, idle time is about one third of the total running time.

In assessing the efficiency of the system we have concluded that in our case, and starting with a semiautomated system, adding the computer has resulted in a factor of 8-10 improvement in the data collection and reduction rate. Moreover, finer scanning and more reduction and manipulation of the data are practical. The investigator also is freed from supervising and operating the system. Maskell[9] has reported very similar measurements using a nulling five-hole probe behind a straight wing. He reported that when the system was working well, the measurements were being made at the rate of about 3 min per data point (as compared to 16 points reduced and plotted for our system, including probe return time).

The program, in its present state, can calculate, on-line, the corrected velocity vector and its components V_x, V_y, V_z, the total pressure loss coefficient, and the circulation distribution (vorticity). On-line plotting of the total pressure loss or streamwise vorticity contours, the velocity vector in the crossflow plane, the spanwise distribution of circulation, and, of course, the variation of any of the measured components with distance, is possible. However, because only two digital-to-analog channels are available, corresponding to x and y position of a display system, the $x-y$ plotters have to be driven in parallel and their pen position (up/down) controlled to plot selectively different results. Great care is required in

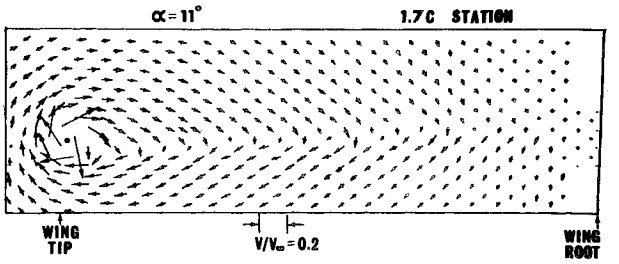

Fig. 13 Velocity vector in crossflow plane for $\alpha = 11°$, 0.35b station.

the plotting subroutines to minimize the delay time required to match the $x-y$ plotter's response.

III. Results

This paper is not intended for the presentation of detailed results but rather for the description of the technique used and the precautions taken. Some typical sample results are, however, presented to demonstrate the capability of the system. Figure 11 shows the contours of equal total pressure loss coefficient, 1.7 chord lengths downstream of the main wing trailing edge, for two angles of attack, 11° and 12.8°. The measurements extend as far outboard as to cover the viscous wake; inboard measurements could be made as close as ⅛ in. to the test section sidewall (wingroot). For $\alpha = 11°$, a part of the wall boundary layer also is scanned and is shown in Fig. 11. The region of the wing wake wall boundary-layer interaction is very small (<0.05 $b/2$); indicating that the wingroot suction system is working properly.

Another feature that is displayed in Fig. 11 is the large difference in the flowfield, near the wingtip, between $\alpha = 11°$ and 12.8°. There does not seem to be a rolled-up region near the tip, for 12.8°, but rather a large region of high total pressure loss. Surface flow visualization, on the wing upper surface, has indicated a region of leading-edge separation near the tip (over about 0.3 $b/2$), for the 12.8° case. The large region of high total pressure loss is the result of this separation. Other flow parameters (vorticity distribution and induced crossflow velocities) also show a sudden variation, as compared to the $\alpha = 11°$ case, as a result of this separation. The lifting characteristics, however, have not shown such a dramatic change. Naturally there is a nonlinear loss of overall lift coefficient ($c_L = 0.734$ for $\alpha = 11°$ and 0.771 for $\alpha = 12.8°$); however, the chordwise loading still shows a large suction peak and would not indicate, by itself, a leading-edge separation (interested readers are referred to Refs. 3 and 4 for detailed description of the wing loading). An important conclusion is that great care must be taken in examining the boundary layer and the nature of its separation for proper understanding of the flowfield and the early phase of roll-up. Realizing that most test facilities[10-14] that are active (or were active) on the trailing vortex problem have a Reynolds number based on mean chord ranging between $0.15-0.85\times10^6$, one would question conclusions drawn from such tests made at large angles of attack.

Sample contours of equal streamwise vorticity are shown in Fig. 12 for $\alpha = 11°$ at 0.35 and 2.5 span station. These contours demonstrate the accuracy and resolution of the sytem. They are obtained using first-order differences from the velocity data, directly without fairing. By integrating the streamwise vorticity distribution it is possible to calculate the spanwise distribution of circulation. From measurements made at four angles of attack, 5°, 8°, 11°, and 12.8°, it is possible to account for 0.85 to 0.99 of the shed vorticity from the wing. Moreover, up to five spans downstream the vortex has not rolled up fully, confirming the author's earlier findings[3-5] from limited scans, and without, at that time, vorticity distributions.

Vectorial presentation of the induced velocities in the crossflow plane is presented in Fig. 13. The figure looks like a tuft grid and serves more as a flow visualization.

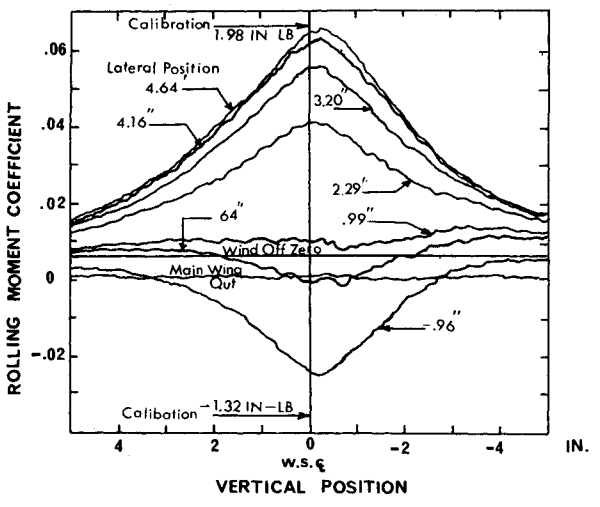

Fig. 14 Induced rolling moment on straight wing $\alpha = 11°$, 2.5*b* station.

Variation of rolling moment coefficient on the small trailing wing with vertical position in the test section, for various lateral stations, is shown in Fig. 14, copied directly from the $x-y$ plotter output. As indicated before, a main wing out traverse also is run to remove irregularities of the undisturbed airstream and model wing manufacturing errors. This zero reference rolling moment coefficient is about 0.006 or 10% of the maximum induced value. It is believed that, if similar precautions were taken, some of the discrepancies noticed between measurements in different test facilities,[14] for an exactly similar generator and trailing model at the same R_c, could be eliminated or reduced. The high resolution of the roll balance system, apparent from Fig. 14, demonstrates that vortex meander does not represent a problem in this test facility (scanning rate is 2 in./min, natural frequency in roll is about 20 Hz). In contrast, in most other test facilities[14-17] it is only possible to measure the maximum induced rolling moment, through long-time observation at different positions, because of vortex meander.

IV. Conclusions

1) A completely computer-controlled wind-tunnel test facility with on-line data collection, reduction, and plotting made detailed and accurate flow surveys behind a sweptback wing at several angles of attack and downstream stations feasible. As a result it was possible to account for almost all of the vorticity shed from the wing and clearly show that the roll-up is neither complete nor in an axisymmetric form at least within five spans downstream.

2) Total pressure loss and streamwise vorticity contours, the velocity vector in the crossflow plane, and circulation distribution can all be mechanically plotted, on-line, and with minimum supervision, thus completely freeing the investigator. Since all data reduction and plotting is done on-line, many more data and finer spacing can be used.

3) A complete set of measurements of the mean flow behind a sweptback wing is now available. These include detailed loading on the generating wing, detailed flowfield properties as well as induced rolling moments on trailing wings. The measurements are believed to be reliable and accurate because of the extra care taken in the design, data collection, and reduction.

4) The use of a conical five-hole probe made calibration of the probe, and the consequent memory required to store the calibration data a simple task. The probe also could be used over a wider range with still adequate accuracy.

5) A careful examination of the effect of the probe support system on the probe reading is recommended for high-accuracy data.

Acknowledgment

This research was supported by the National Research Council of Canada, Grant A7799, and by Lockheed Georgia Company, Contract CK 27059P. The authors would like to acknowledge the assistance of D. Earl during the early phases of the development of the computer system.

References

[1]Olsen, J., Goldberg, A., and Rogers, M., (Eds.), *Aircraft Wake Turbulence and its Detection*, Plenum Press, New York, 1971.

[2]El-Ramly, Z., "Aircraft Trailing Vortices: A Survey of the Problem," Carleton University, Rept. No. ME/A 72-1, Nov. 1972, p. 186.

[3]El-Ramly, Z., Rainbird, W. J., and Earl, D. G., "Some Wind-Tunnel Measurements of the Trailing Vortex Development Behind Sweptback Wing: Induced Rolling Moment on Intercepting Wings," AIAA Paper 75-884, Hartford, Conn., June 16-18, 1975.

[4]El-Ramly, Z., "Investigation of the Development of the Trailing Vortex System Behind a Sweptback Wing," Carleton University, Rept. No. ME/A 75-3, Oct. 1975, p. 187.

[5]El-Ramly, Z. and Rainbird, W. J., "Wind-Tunnel Measurements of the Trailing Vortex Development Behind Sweptback Wing: Effect of Simulated Jet Engines on the Flowfield," AIAA Paper 76-63, Washington, D. C., Jan. 26-28, 1976.

[6]Rainbird, W. J., "Design and Use of Boundary Layer Control for 2D Aerofoil Testing, NAE 15 in. × 60 in. Section," National Research Council, Canada, Lab. Memo No. HSA-40, Feb. 1970.

[7]Wickens, R., South P., Rangi, R. S., and Henshaw, D., "Experimental Development in V/STOL Wind Tunnel Testing at the National Aeronautical Establishment," *Canadian Aeronautics and Space Journal*, Vol. 19, April 1973, pp. 145-154.

[8]Corsiglia, V. R., Schwind, R. G., and Chigier, N. A., "Rapid Scanning, Three-Dimensional Hot-Wire Anemometer Surveys of Wing-Tip Vortices," *Journal of Aircraft*, Vol. 10, Dec. 1973, pp. 752-757.

[9]Maskell, E. C., "Progress Towards a Method for the Measurement of the Components of the Drag of a Wing of Finite Span," Royal Aircraft Establishment, Farnbourough, England, TR 72232, Dec. 1972.

[10]Logan, A. H., "Vortex Velocity Distributions at Large Downstream Distances," *Journal of Aircraft*, Vol. 8, Nov. 1971, pp. 930-932.

[11]Grow, T. L., "Effect of Wing on its Tip Vortex," *Journal of Aircraft*, Vol. 6, Jan.-Feb. 1969, pp. 37-41.

[12]Marchmann, III, J. F. and Marshall, J. R., "Vortex Age as a Wake Turbulence Scaling Parameter," AIAA Paper 74-76, Washington, D. C., Jan. 30-Feb. 1, 1974.

[13]Chigier, N. A. and Corsiglia, V. R., "Wing-Tunnel Studies of Wing Wake Turbulence," AIAA Paper 72-41, San Diego, Calif., Jan. 17-19, 1972.

[14]Stickle, J. W. and Kelly, N. W., "Ground-Based Facilities for Evaluating Vortex Minimization Concepts," *NASA Symposium on Wake Vortex Minimization*, Washington, D. C., Feb. 25-26, 1976.

[15]Rossow, V. J., Corsiglia, V. R. and Phillippe, J. J., "Measurements of the Vortex Wakes of a Subsonic and a Supersonic-Transport Model in the 40- by 80- Foot Wind Tunnel," NASA TM X-62.391, Sept. 1974.

[16]Rossow, V. J., Corsiglia, V. R., Schwind, R. G., Frick, J.K.D., and Lemmer, O. P., "Velocity and Rolling-Moment Measurements in the Wake of a Swept-Wing Model in the 40- by 80- Foot Wind Tunnel," NASA TM X-62, 414, April 1975.

[17]Patterson, J. C. Jr., "Vortex Attenuation Obtained in the Langley Vortex Research Facility," *Journal of Aircraft*, Vol. 12, Sept. 1975, pp. 745-749.